

Correlative Micro-Compression and 3D X-ray Nanotomography Study of the Fracture Behavior of TCP Phases in an Additively Manufactured Ni-Base Superalloy

Michael Sommerschuh^{1*}, Janis Wirth¹, Benoit Merle², Julian Pistor³, Silvan Englisch¹, Thomas Przybilla¹, Carolin Körner³, Mathias Göken², Benjamin Apeleo Zubiri¹, and Erdmann Spiecker^{1*}

¹ Institute of Micro- and Nanostructure Research (IMN) & Center for Nanoanalysis and Electron Microscopy (CENEM), Interdisciplinary Center for Nanostructured Films (IZNF), Department of Materials Science and Engineering, Friedrich-Alexander University Erlangen-Nürnberg (FAU), Erlangen, Bavaria, Germany.

² Materials Science & Engineering - Institute I, Interdisciplinary Center for Nanostructured Films (IZNF), Friedrich-Alexander-University Erlangen-Nürnberg (FAU), Erlangen, Bavaria, Germany.

³ Chair of Materials Science and Engineering for Metals (WTM), Friedrich-Alexander-University Erlangen-Nürnberg (FAU), Erlangen, Bavaria, Germany.

* Corresponding authors: michi.sommerschuh@fau.de, erdmann.spiecker@fau.de

Ni-base superalloys are used as turbine blade material in the hot sections of gas turbines because of their superior mechanical stability under high temperature conditions, enabling high gas outlet temperatures, and thus turbine efficiencies [1, 2]. The outstanding mechanical properties are obtained by a two-phase microstructure consisting of L₁₂-ordered γ' -precipitates coherently embedded in a solid solution strengthened fcc γ -matrix [3]. However, the addition of precipitation forming elements like Al and solid solution hardening elements like Re drives these alloys to the brink of phase stability at high temperatures [2, 3]. At application conditions, topologically close packed (TCP) phases form and deteriorate the mechanical properties by a variety of different mechanisms, e.g., consumption of solid solution strengthening elements, disturbance of the local microstructure or crack formation [2]. To comprehend the severity of TCP-phase formation at various temperatures and loading conditions, tensile, creep and fatigue characteristics of conventionally cast Ni-base superalloys have been investigated in literature [4, 5]. However, correlative research linking local and global strain evolution in superalloys with TCP phases is quite fragmentary [6]. In the last years, additive manufacturing of single crystalline Ni-base superalloys, e.g., by selective electron beam melting (SEBM), has been developed offering several advantages over conventional processing routines. An important benefit is the diminution of micro-segregation events of heavy transition metal elements after solidification [7], which govern the propensity of the microstructure to precipitate TCP phases at high temperature exposure [8].

In this contribution, the morphological nature and three-dimensional (3D) distribution of TCP phases in a single crystalline Ni-base superalloy manufactured by SEBM are evaluated and investigated regarding their deformation behavior and precipitate-matrix interaction during micro-mechanical testing.

For that purpose, micro-pillars on bulk support are extracted from an appropriate superalloy sample by laser ablation and subsequently polished by FIB-milling. The pillars are investigated by combining X-ray nanotomography (nano-CT) using a Zeiss Xradia 810 Ultra X-ray microscope and interrupted room temperature micro-compression testing using a KLA-Tencor Nanoindenter G200 with a force resolution of 50 nN working under load control (Figure 1). The lab-based X-ray microscope with a Cr-K α -source (5.4 keV) is equipped with a Fresnel zone plate and provides a resolution of around (50 nm)³ in a field of view of (16 μ m)², which is perfectly suited to examine TCP phases with diameters of several hundreds

of nanometers and lengths of several micrometers (Figure 1a). Moreover, TCP phases can be studied in absorption and Zernike phase contrast imaging mode, since they accumulate heavy elements and supply both a significantly shorter absorption length and a detectable phase shift with respect to the surrounding matrix. By applying this non-destructive 3D imaging approach, the local strain evolution within and around TCP phases leading, e.g., to crack formation (Figure 1c,d), can be investigated stepwise at different strain states by interrupted *in situ* nano-CT. The strain levels, at which tomograms of a pillar have been recorded, comprise 0%, 10%, 20% and 30% global strain. For the intermediate strain levels, no quantitative data is presented here.

With increasing angle θ between the long axis of the TCP phases and the vertical loading direction during micro-compression testing, as indicated in Figure 2a, the resolved straining of the TCP phases changes from compressive to tensile. The curve in Figure 2b is derived from the plastic Poisson ratio (0.66 for a plastic strain of 31 %), which relates the lateral expansion of the pillar to its vertical compression, assuming isotropic deformation behaviour of the pillar material. In the experiments, orientation-dependent deformation effects resulting from the activation of slip bands in the single-crystalline pillar induce a local strain evolution that slightly deviates from this simplified model. Still most TCP phases under tensile strain show brittle fracture and fragmentation (data points indicated with a red cross in Figure 2b, while phases under compressive strain stay intact (filled circles). Figure 2a shows the schematic evolution of a TCP phase, which experiences tensile strain along its long axis. With growing tensile strain, fragments of TCP phases further disintegrate until a certain critical length is reached while the distances between the fragments increase as well.

By combining non-destructive nano-CT and interrupted micro-compression testing, the disintegration of TCP phases under tensile strain and formation of local cracks at the fragments can be confirmed. However, the cracks do not extend into the surrounding matrix (Figure 1 d). This finding hints to a failure mechanism of the microstructure, which is localised at the TCP phases [9].

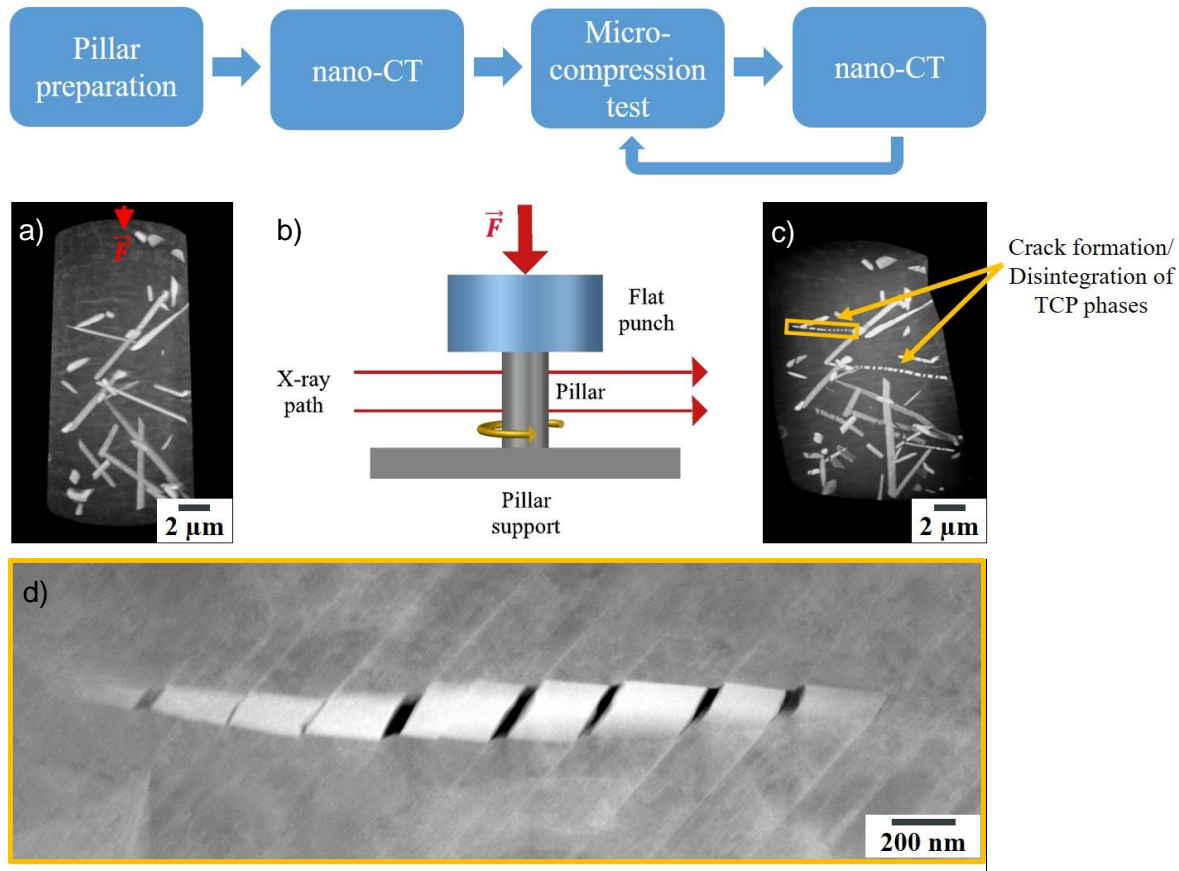
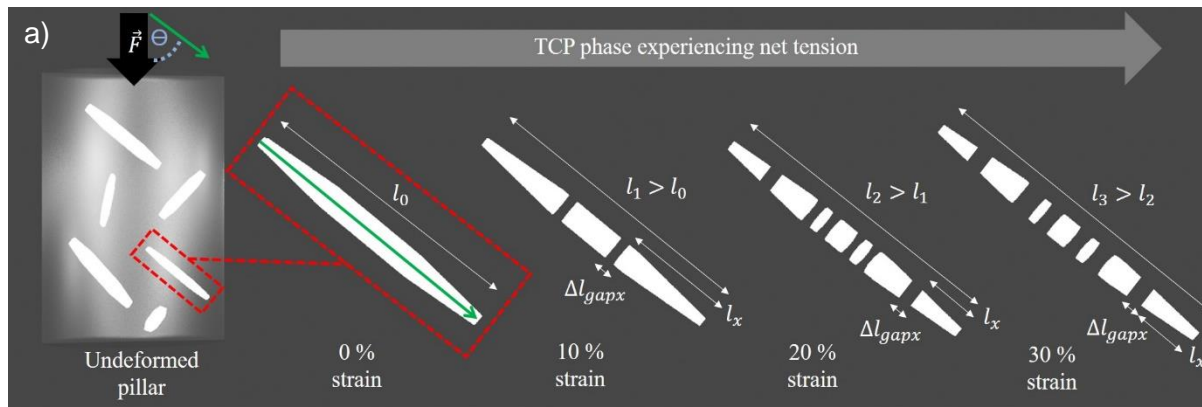


Figure 1. Combined lab-based nano-CT and interrupted micro-compression experiments on a micro-pillar extracted from an additively manufactured Ni-base superalloy: a) Zernike phase contrast nano-CT 3D reconstruction (volume rendering) before micro-compression testing. The TCP phases appear in bright contrast, the applied force direction of micro-compression test is indicated by red arrow. b) Schematic of the geometry of the interrupted micro-compression test and subsequent nano-CT investigation performed for several compression steps. c) Exemplary 3D reconstruction of the micro-pillar from a) after compression to 31% strain. TCP phases with close to horizontal orientation show tensile (brittle) fracture as result of lateral expansion of the pillar (plastic Poisson effect). d) Scanning transmission electron microscopy high angle annular dark field image of the TCP phase outlined in c). Cracks between TCP phase fragments appear in dark contrast.



b)

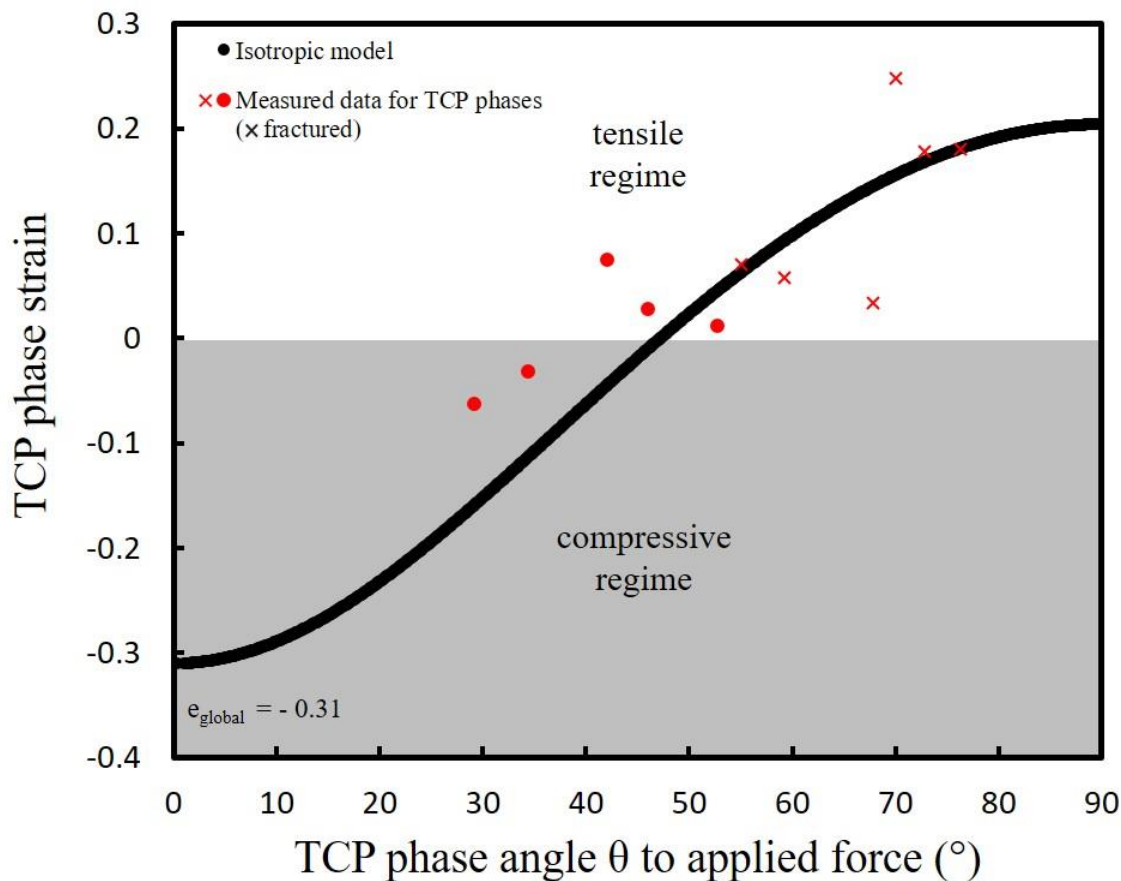


Figure 2. Schematic interpretation and experimental straining behaviour of TCP phases upon micro-compression testing: a) Schematic representation of the strain evolution of a TCP phase experiencing net tension along its long axis (marked green). θ delineates the angle of the long axis of TCP phases towards the compression force direction \vec{F} . l_0 , l_1 , l_2 and l_3 denote the length of the whole TCP phase at 0%, 10%, 20% and 30% global strain, respectively, while l_x and Δl_{gapx} denote the length of a fragment and of a gap between two fragments formed during compression of the pillar. b) Measured local strain of TCP phases (red data points) after pillar compression to 31% global strain (e_{global}) depending on the

angle θ . TCP phases, which have fragmented during pillar compression, are marked with red cross. The black curve shows the expected strain values calculated under the assumption of isotropic deformation behaviour of the pillar material (for plastic Poisson ratio of 0.66 at a global plastic strain of 31 %).

References:

- [1] RC Reed in "The Superalloys: Fundamentals and Applications" (2006) p. 1.
- [2] AS Wilson, *Materials Science and Technology* **33**(9) (2017), p. 1108.
- [3] B Geddes, H León and XM Huang in "Superalloys: Alloying and Performance" (2010).
- [4] A Cervellon et al., *Acta Materialia* **188** (2020), p. 131.
- [5] K Hrutkay and D Kaoumi, *Materials Science and Engineering A* **599** (2014), p. 196.
- [6] P Caron, *Materials Science & Engineering A* **254**(1-2) (1998), p. 1.
- [7] M Ramsperger, RF Singer and C Körner, *Metallurgical and Materials Transactions A* **47**(3) (2016), p. 1469.
- [8] J Pistor and C Körner, *Materials Letters: X* **1** (2019), p. 100003.
- [9] We gratefully acknowledge financial support by the German Research Foundation (DFG) within the frameworks of the research training group GRK1896 "In situ Microscopy with Electrons, X-rays and Scanning Probes", the project SP648/8 "High-resolution X-ray microscopy for correlative tomography, high throughput screening and in situ mechanical testing of structural and functional materials" (project number 316992193) and the projects A6, A7 and B2 of the collaborative research center SFB Transregio/103 "From Atoms to Turbine Blades - a Scientific Approach for Developing the Next Generation of Single Crystal Superalloys" (project number 190389738).